Journal of Electronic Materials (2023) 52:5178–5188
https://doi.org/10.1007/s11664-023-10534-3

TOPICAL COLLECTION: 19TH CONFERENCE ON DEFECTS (DRIP XIX)

Investigation of Doping Processes to Achieve Highly Doped Czochralski Germanium Ingots

Aravind Subramanian[1] · Nikolay Abrosimov[1] · Alexander Gybin[1] · Christo Guguschev[1] · Uta Juda[1] · Andreas Fiedler[1] · Florian Bärwolf[2] · Ioan Costina[2] · Albert Kwasniewski[1] · Andrea Dittmar[1] · R. Radhakrishnan Sumathi[1]

Received: 1 December 2022 / Accepted: 30 May 2023 / Published online: 22 June 2023
© The Author(s) 2023

Abstract

Highly doped germanium (HD-Ge) is a promising material for mid-infrared detectors, bio-sensors, and other devices. Bulk crystals with a doping concentration higher than 10^{18} cm^{-3} would be desirable for such device fabrication technologies. Hence, an effective method needs to be developed to dope germanium (Ge) ingots in the Czochralski (Cz) growth process. In this study, a total of 5 ingots were grown by the Cz technique: two undoped Ge ingots as a reference and three doped ingots with 10^{18}, 10^{19} , and 10^{20} atoms/cm^3 respectively. To obtain a uniform *p*-type doping concentration along the crystal, co-doping of boron-gallium (B-Ga) via the Ge feed material was also attempted. Both B and Ga are *p*-type dopants, but with a large difference in their segregation behavior (contrary segregation profile) in Ge, and hence it is expected that the incorporation of dopants in the crystal would be uniform along the crystal length. The distribution of the dopants followed the Scheil-predicted profile. The etch pit density maps of the grown crystals showed an average dislocation density in the order of 10^5 cm^{-2}. No increase in the overall etch pit count was observed with increasing dopant concentration in the crystal. The grown highly doped Ge crystals have a good structural quality as confirmed by x-ray diffraction rocking curve measurements.

Keywords Highly doped germanium · dopant diffusion · structural analysis · doping methods and bulk ingots

Introduction

There has been renewed interest in the search for new materials for plasmonic nano-antennae for nano-optical applications. Directing and concentrating the incoming electromagnetic into sub-diffraction-limited near-field volumes makes it possible to access the "fingerprint" wavelength region between 5 and 15 μm in the mid-infrared (MIR) spectrum.[1–3] This region is of great interest as the earth's atmosphere is relatively transparent and contains characteristic vibrations of many molecules. The applications with such a photonic system would enable communication technologies, environmental and biochemical sensing, industrial process control, detection of toxins, and point-of-care diagnostics.[4,5] Recently, highly doped semiconductors have been proposed as tuneable materials for MIR applications.[4–6] Compared to the currently used metals, such as Au, Ag, and Al, highly doped Ge possesses a much lower plasma frequency.[4,6] However, the free carrier concentration can be regulated by doping germanium (Ge) (*n*-type or *p*-type) with the desired doping levels, and further tuned by methods such as optical excitement.[4] Furthermore, considering the compatibility of Ge with the widely used silicon (Si)-based CMOS fabrication, losses related to lattice misfits could be effectively addressed with a higher doping level (10^{19}–10^{20} cm^{-3}) and a tuneable frequency up to 95 THz corresponding to 3.1 μm.[1] Such a nano-antenna fabricated on a Si substrate is shown in Fig 1.[7] In the case of Ge, highly doped substrates are currently mainly produced using epitaxial and ion implantation methods with doping levels of > 10^{19} cm^{-3}.[4,8] Considering the increased demand for such devices in the future, a combination of efficient device fabrication technologies, such as wafer-bonding, transfer-printing of Ge on Si, etc., would necessitate highly doped germanium (HD-Ge) bulk crystals (i.e., ingots), which could meet the needs of producing higher-quality plasmonic material.

✉ R. Radhakrishnan Sumathi
radhakrishnan.sumathi@ikz-berlin.de

[1] Leibniz-Institut für Kristallzüchtung (IKZ), Max-Born-Str. 2, 12489 Berlin, Germany

[2] Leibniz-Institut für innovative Mikroelektronik (IHP), Im Technologiepark 25, 15236 Frankfurt (Oder), Germany

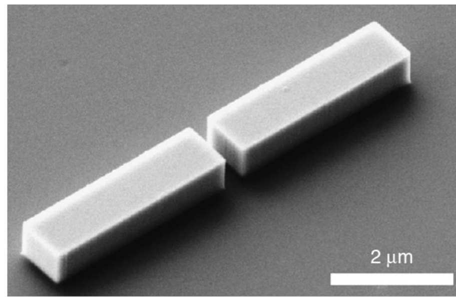

Fig. 1. SEM image of a single Ge double-rod antenna on a silicon substrate with a 3.5-μm arm length. Reproduced from Ref. 7, under a Creative Commons attribution 4.0 international.

The properties of the grown crystals need to be uniform for any device application. However, the non-uniformity, the presence of structural defects, and mainly small angle grain boundaries (SAGBs) even with low doping concentrations will deteriorate the devices. At higher doping levels, a larger number of crystal defects might be introduced in the crystal. Crystal defects induced by unstable growth conditions and varying parameters might also cause different impurity distributions. Inappropriate melt mixing or a faster growth rate has a fatal effect on the structural quality. For instance, the agglomeration of dopants in a dislocation or a grain boundary may result in inhomogeneous material. Hence, it is important to investigate the segregation of the dopants, while the optimization of the crystal growth parameters would be important to bring about the highly doped Ge ingots.

We report the challenges associated with achieving high doping levels in Ge grown by the Czochralski (Cz) method (Cz-Ge) ingots. A lower number of crystal defects (dislocations ~ 10^5–10^6 cm^{-2}) in the Cz-Ge ingots, compared to the Ge-Si epi-layers (dislocations ~ 10^6–10^8 cm^{-2}), can be achieved. Substrates from such ingots could further reduce the intrinsic losses in the fabricated MIR detector.[4] Achieving high doping levels in bulk-grown Ge is challenging, mainly due to a lack of effective doping means and methods. Previous studies showed that, while growing CZ-Ge with doping concentrations higher than 10^{19} cm^{-3}, the crystal–melt interface stabilities were prominent .[9] Recently, Sumathi et al. reported the growth of heavily doped *n*-type Cz-Ge ingots with dopant concentrations up to 3×10^{18} cm^{-3} using the gas-phase doping method.[8] Some of the factors that limit the ease of producing such ingots are[8,9]:

- Solubility limit of major dopants in Ge
- Limitation due to low and high segregation coefficient (k_0 <<1 or k_0>> 1).
- Constitutional supercooling
- Introduction of structural defects.

Table I Feedstock weight and doping concentrations discussed in this work

Crystal name	Crystal weight (g)	Initial doping concentration (atoms/cm^3)	Dopant atoms
Ref-Ge_1	860	$< 10^{15}$	–
HD-Ge_1	860	10^{18}	Ga
HD-Ge_2	860	10^{19}	B-Ga
Ref-Ge_2	500	$< 10^{15}$	–
HD-Ge_3	500	10^{20}	Ga

Among the different dopants and doping methods, we have studied the effects related to introducing Ga and B dopants with varying concentrations (10^{18}–10^{20} cm^{-3}) with or without co-doping in Ge. Ga was selected as the dopant due to its stability in the solid phase to carry out solid-dopant doping, and its high solubility in Ge (5×10^{20} cm^{-3}).[10]

Experimental

Crystal Growth

The Ga-doped germanium ingots were grown using the Cz method. Electronic-grade polycrystalline Ge was used as the feedstock for all the Ge crystals grown in this work.

A total of five ingots were grown, with two reference ingots and three ingots with varying dopant (Ga) concentrations (Table I). A Ge seed crystal of <100> orientation was used for the growth experiments. The crystals were grown in an argon atmosphere at a pressure of about 40 mbar. The Ar flow rate was 13 Nl/min. Furthermore, all the crystals in this work were grown with the same constant growth rate of 30 mm/h. Before the growth experiment, the Ge feedstock was etched using an HF:HNO_3 (3:1) solution (approx. 5 min) to remove oxides at the surface. After this procedure, the feedstock was loaded into a graphite crucible in a furnace. The crucible and the seed crystal were rotated in counter directions at 6 and 10 rpm, respectively. A resistively heated furnace was used for the growth experiments. Figure 2a depicts the prominent parts of the Cz equipment.

Doping

As mentioned in Sect. "Introduction", to address a major challenge in growing HD-Ge ingots, i.e., an effective doping method, solid-dopant doping with a different scheme was carried out in this work. Furthermore, co-doping was also attempted in HD-Ge_2. 5N pure metallic Ga and B powders were used for doping. Such co-doping in this melt growth technique was carried out by adding B and Ga to the Ge feedstock by introducing them simultaneously via dopant

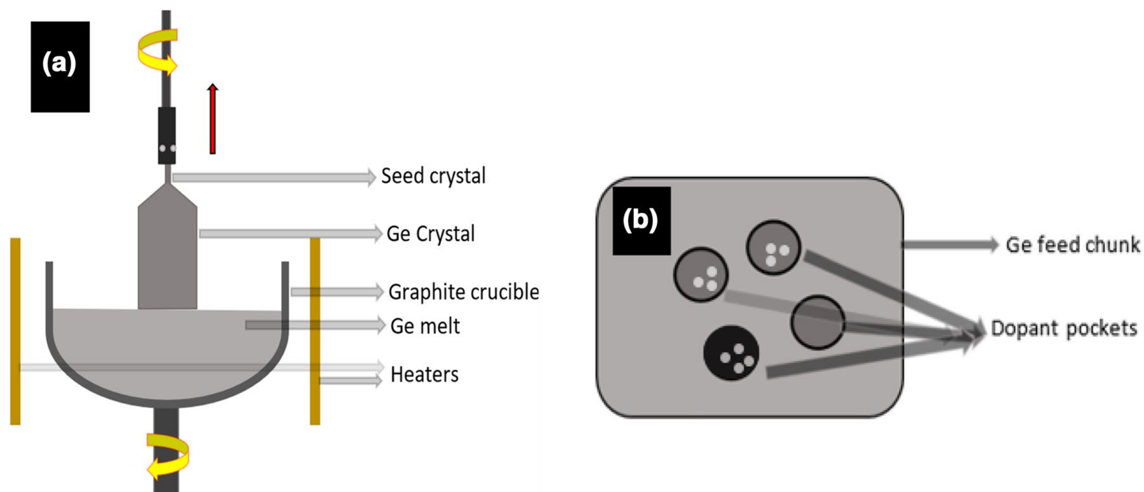

Fig. 2. (a) Schematic of a standard Cz process, (b) schematic of the dopant pockets used to carry out solid-dopant co-doping: (B: $C_0 \approx 10^{19}$ cm^{-3} and Ga: $C_0 \approx 10^{19}$ cm^{-3}).

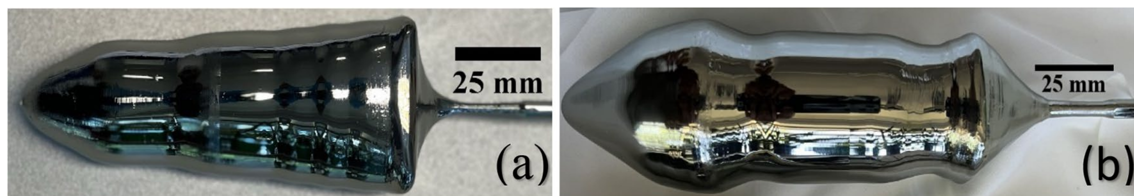

Fig. 3. (a) HD-Ge_2: co-doped Ge ingot with dopants B and Ga ($C_{0(Ga)}$ and $C_{0(B)} \approx 10^{19}$ cm^{-3}), (b) HD-Ge_1: Ga-doped Ge ingot ($C_{0(Ga)} \approx 10^{18}$ cm^{-3}).

"pockets", as shown in Fig 2b. The segregation coefficients of Ga and B in Ge have been reported to be 0.087 and 5–6, respectively.[10,11] Considering such high segregation of B and very low segregation of Ga, the active carrier concentration in the co-doped ingot would be thought to be relatively constant throughout the ingot length. To limit the loss of dopants due to evaporation, the pockets were sealed with Ge feed particles (Fig. 3).

Characterization

The grown crystals were 85–100 mm long with a diameter between 35 and 45 mm, and were grown with a growth rate of 30 mm/h. The grown ingots were cut in the middle along the [100] direction. Subsequently, wafers with 2-mm thickness were cut perpendicular to the growth direction from the first half of the vertical cut. From the other half, a long cut along the axial direction was carried out, such that the (110) face was exposed along the ingot length (i.e., cross-section sample). The (110) wafers were 35- to 40-mm-diameter semi-circles and were polished using the standard chemo-mechanical polishing procedure for Ge. The high doping concentration resulted in a polycrystalline region at the tail/cone end of the doped ingots. Furthermore, the "thread-like" structures observed at the cone end of the highly doped ingot are due to the rapid solidification of the dopant oversaturated melt (Fig 4). This effect was observed in all the investigated crystal growth experimental profiles. The other introduced

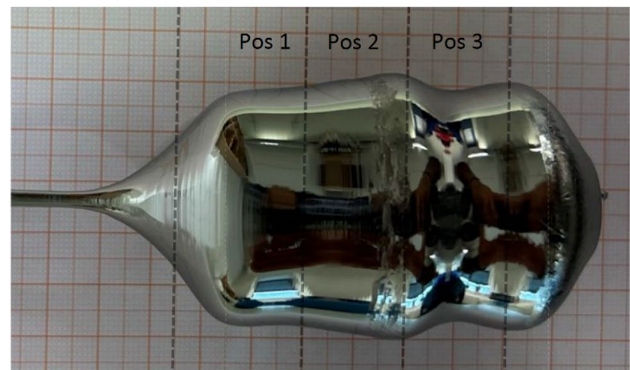

Fig. 4. HD-Ge_3 [$C_o \approx 2 \times 10^{20}$ cm^{-3}] ingot, *Pos 1* (25 mm), *Pos 2* (45 mm), and *Pos 3* (65 mm) correspond to the different regions along the crystal length from where wafers for EPD and XRD-rocking curve measurements were carried out. Similar positions were used for samples from all the crystals.

structural inhomogeneities, such as dislocations and SAGBs due to the high concentration of dopants, were also examined. Identifying these structural defects and correlating these effects with the growth parameters is important in the preparation of higher-quality HD-Ge ingots. The microstructure was analyzed by checking the etch pit density (EPD) maps, carrying out x-ray diffraction (XRD) rocking curve measurements and energy dispersive Laue spectroscopy (EDLM). The EDLM method is a relatively new technique for the non-destructive identification of SAGBs,[12] especially in the lower regions of the grown ingots, due to the after effect of dopant segregation and a high number of etch pits (dislocations). The EDLM mapping was carried out using a commercial tool. The EPD analysis was done by using wet chemical etching with a solution containing hydrofluoric acid, nitric acid, and copper nitrate.[13] The dopant segregation profile was reviewed using inductively coupled plasma optical emission spectroscopy (ICP-OES), atomic absorption spectroscopy (AAS), secondary ion mass spectroscopy (SIMS), and micro-x-ray fluorescence (μ-XRF). μ-XRF was carried out under low-vacuum conditions (1–20 mbar) using a Bruker M4 TORNADO spectrometer. The Rh x-ray source was operated at a voltage of 50 kV and the tube current was set to 200 μA and point measurements were performed. The measurement time per point was set to 100 s. Quantification was conducted by using the fundamental parameter approach based on Sherman's equation.[14] The resistivity and the active carrier concentration were determined using a 4-point probe and the Hall measurement at room temperature (RT), respectively.

Results and Discussion

Microstructural Analysis of HD-Ge Ingots

The microstructural characterization of the grown Ge ingots analyzed by the EPD maps and EDLM measurements are presented here. The etch pit counts were carried out separately at the center, middle, and periphery surface areas (see Fig. 5). Wafers were obtained from three positions along the length of the ingot, as marked in Fig. 4, namely, the seed end, the middle region, and the cone end. As expected, dislocation counts increase at the periphery of the crystal and along the ingot height (Fig. 5a). This could be due to the thermal stresses acting on the growing ingot, while the effect of dopants is limited.[15,16] The usual "ring-like" pattern[15] was seen upon observing the etch pit distribution within the wafers in the radial direction. The etch pit map of one of such wafers obtained from the middle bulk (approx. crystal

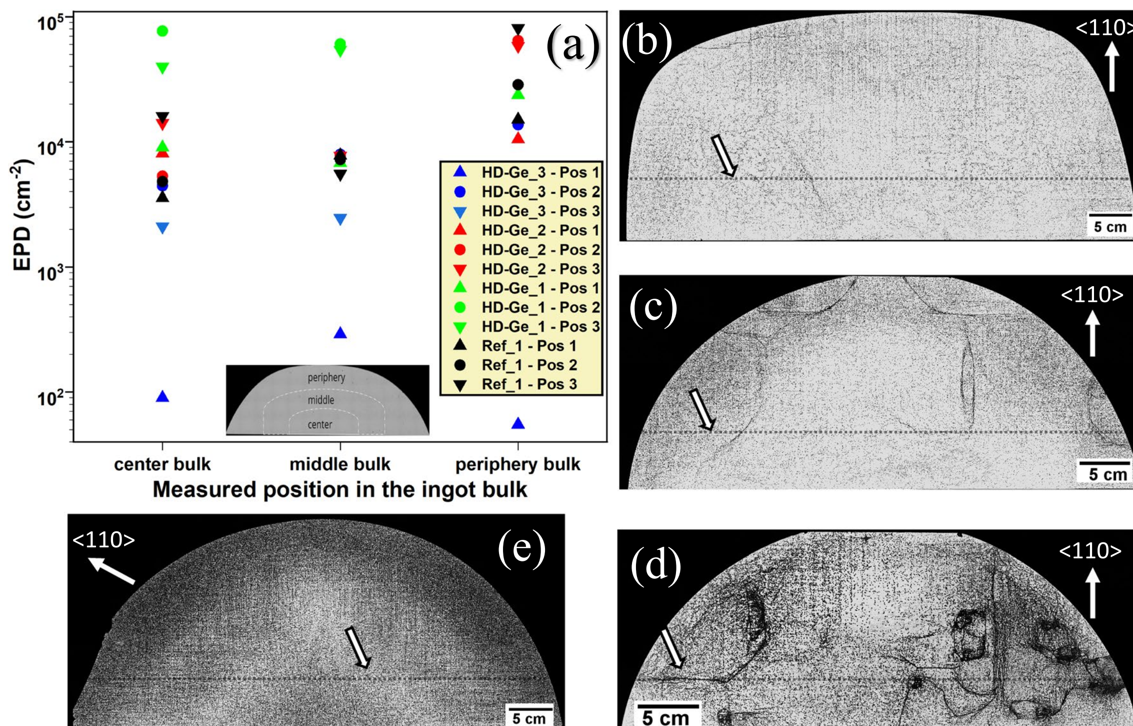

Fig. 5. (a) EPD counts of ingots, Ref-Ge 1, HD-Ge_1, HD-Ge_2, and HD-Ge_3 represented in a log scale, (b) etch pit map of the middle region (crystal length 30–60 mm) of ingot HD-Ge_1, (c)), (d), and (e) etch pit maps showing clustering of dislocations of the seed end (crystal length 5-25 mm), middle region (crystal length 30–60 mm), and the cone end (crystal length 70–90 mm) of ingot HD-Ge_2, respectively. The horizontal dotted line in (c)–(e) represents where the XRD-RC was performed.

length 40 mm) of the HD-Ge_1 is shown in Fig. 5b, where the ring-like pattern can also be seen. Furthermore, a uniform distribution of etch pits was observed in the ingot. The higher number of dislocations revealed by the EPD maps of HD-Ge_1 could be due to the mechanical strain induced in the crystal due to the thermal stress, possibly during cooling.[16] No clear effect in the overall dislocation density was observed with increasing dopant concentrations.

A higher number of dislocation clusters were observed along the axial length of the ingot HD-Ge_2 (Fig 5c, d, and e). The presence of dislocation clusters (Figs. 5c, d, and e, and a) was prominent with increasing doping concentration along the length of this crystal. Furthermore, many of the etch pits were observed to be overlapping with one another. This might result in a lower count of etch pits than the actual number (Fig. 6b). The etch pits observed using a higher magnification revealed an inverted pyramid structure of the pits with its edges along the [110] direction. This is because the dislocations in Ge crystal grown along the [100] direction move along the {110} planes in the [111] direction.

Figure 7 shows the EDLM maps obtained for the doped ingots. The mappings were recorded at a tube current of 600 μA to detect high-intensity Bragg peaks to qualitatively assess the microstructural features. For these mappings, the

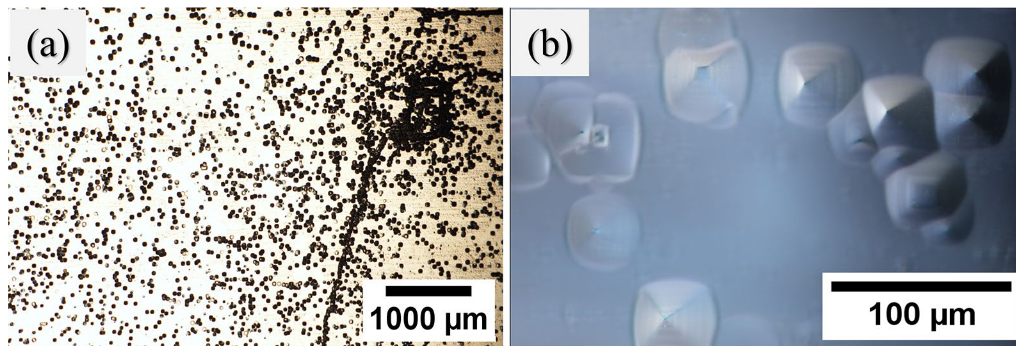

Fig. 6. Etch pits observed in one of the sample surfaces of HD-Ge_2: (a) dislocation cluster, (b) magnified (x50) image of the etch pits shown in (a).

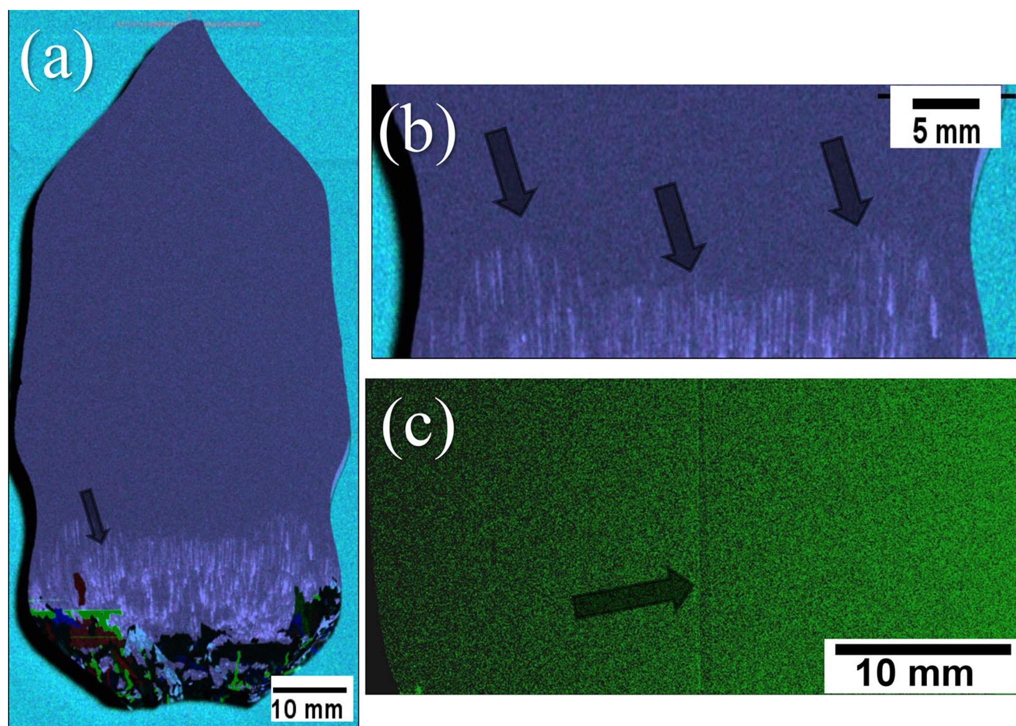

Fig. 7. EDLM mapping results of the ingots: (a) HD-Ge_3–crystal length cross-section (C_0 ~ 10^{20} cm^{-3}), (b) HD-Ge_3 (C_0 ~ 10^{20} cm^{-3}), ingot length 45–60 mm, and (c)) HD-Ge_2 (C_0 ~ 10^{19} cm^{-3}), ingot length 60–70 mm.

integration time per point was set to 20 ms and the spots were measured 3–4 times to increase the counting statistics, i.e., the scans involved 3–4 passes over the sample. The distance between individual points was between 27 and 65 μm. Due to sample damage, the entire length of the HD-Ge_2 could not be carried out. However, the bottom region of the ingots (crystal length 60–80 mm) has been compared, which is of more interest. The compared regions of the ingots are depicted in Fig. 7c.

SAGBs (marked in HD-Ge_3; Fig. 7b) corresponded to the highest doping concentration along the crystal length in the mono-crystalline region. Furthermore, a sub-grain boundary was also identified by the EDLM in HD-Ge_2 and is marked in Fig. 7c. Upon investigating this region under the microscope, a micro-scratch was observed. Hence, it remains to be further investigated whether the observed "sub-grain boundary" is an artefact or a structural defect. The region that demarcates between SAGB-free and defected regions (marked with a black arrow in Fig. 7a) does not correspond to the start of the polycrystalline Ge at the bottom of the ingot. The bottom region of the EDLM map of HD-Ge_3 depicts the polycrystalline region due to dopant over-saturation. The dark regions (contrast in brightness) seen in the EDLM at the bottom of HD-Ge_3 (Fig 7a) are due to the different orientations of the poly-grains compared to the mono-crystalline bulk.

X-ray diffraction rocking curve (XRD-RC) analysis was also carried out on the grown (see Fig. 8) ingots at similar positions marked in Fig. 4. The position of the horizontal line scan to obtain the rocking curve is marked in Fig. 5c, d, and e. The

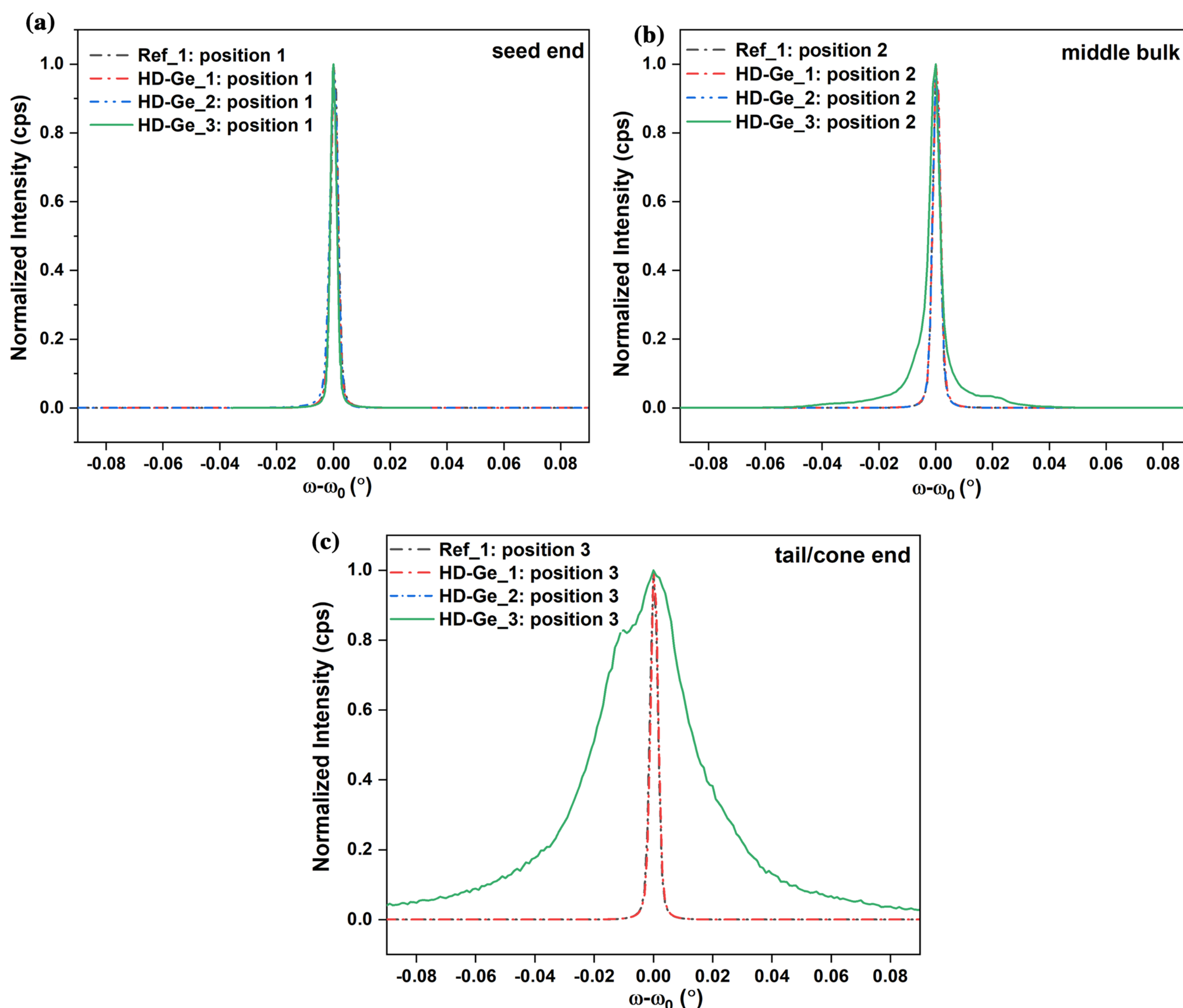

Fig. 8. XRD-rocking curve measurements of ingots Ref-Ge 1, HD-Ge_1, HD-Ge_2, and HD-Ge_3: (a) seed end ingot length 20–25 mm, (b) middle bulk ingot length 45–55 mm, and (c)) tail/cone end ingot length 55-65 mm.

measurements were carried out using the symmetric (400) reflex. The full-width half-maximum (FWHM) obtained for the ingots, Ref 1, HD-Ge_1, and HD-Ge_2 was around 9 arcsec, indicating a good quality of the grown crystals. On comparing the EPD of HD-Ge_3 (Fig. 5a) with the measured rocking curve at position 2, the broadening of the peak along the crystal length could be mainly due to the introduction of many SAGBs. However, the EDLM at position 2 (Fig. 7a) did not show any presence of SAGBs. Hence. the SAGBs present in this region could be less than 2.5°, which is lower than the sensitivity of the EDLM technique. Furthermore, the FWHM measured at position 3 (Fig 8c) confirms the findings by the EDLM (Fig 7b). suggesting the presence of a large number of SAGBs.

Impurity concentration in the grown ingots

The resistivity profile in the grown ingots was initially checked using the 4-point probe method. From the resistivity values obtained, the dopant/impurity concentration was calculated using theoretically derived mobility values.[17] The segregation profiles were calculated using the Scheil equation, assuming the equilibrium segregation coefficient of dopants (k_0 (Ga) ≈ 0.087).[11] The effective segregation coefficients (k_{eff}[calc.]) were calculated using,

$$k_{eff} = \frac{k_0}{k_0 + (1 - k_0)\exp\left(\frac{-v\delta}{D}\right)}$$

where v is the growth rate of the crystals, δ is the diffusion layer thickness, and D is the diffusivity of dopants in Ge.[18] The diffusivity values considered were, for Ga in Ge, 7.2 $\times 10^{-5}$ cm^2/s, and for B in Ge, 1.4 × 10^{-4} cm^2/s.[10,11,19] The calculated k_{eff}[calc.] of Ga and B in Ge in this work were 0.148 and 2.581, respectively. The obtained values for the k_{eff}[calc.] of Ga in the growth experiments are in good agreement with previously obtained values for Ga in Ge crystals at growth rates of around 30 mm/h. The effective segregation of Ga in Ge is shown to increase at higher growth velocities.[20,21] Similarly, for B in Ge, the K_{eff}[calc.] obtained did not deviate much from the previously reported K_{eff} values for B in Cz-Ge crystals.[22] However, the experimentally estimated segregation of B in co-doped Ge is very low due to the interaction of Ga and B. The chemical concentrations of dopants were measured using AAS, ICP-OES, μ-XRF, and SIMS techniques. Figure 9 shows the results from the 4-point probe measurements on ingots HD-Ge_2 and HD-Ge_3. The resistivity measurement of the co-doped ingot (HD-Ge_2) follows the theoretical curve of Ga and did not show the presence of B. The theoretically calculated resistivity due to B-segregation is also shown in Fig. 9a.

Considering the high segregation coefficient of B in Ge, it was expected that lower resistivities in the top region of the ingot HD-Ge_2 would be obtained due to the co-doping of B and Ga. On the contrary, a similar trend of the resistivity profile in HD-Ge_2 as in the gallium-doped HD-Ge_3 was observed (Fig. 9b). Hence, the higher resistivity values that were measured in the top region of the B-Ga co-doped ingot are only influenced by the Ga segregation. The distribution of Ga in HD-Ge_1 and HD-Ge_2 along with B in the HD-Ge_2 was checked using AAS, ICP-OES, SIMS, and the Hall measurements at RT. The B concentration in the ingot could not be detected by ICP-OES and AAS measurements due to the light weight of B and the formation of B_4C, respectively. However, the measured Ga distribution in the ingots followed a Scheil-like dopant distribution trend. From Fig 10a, the highest

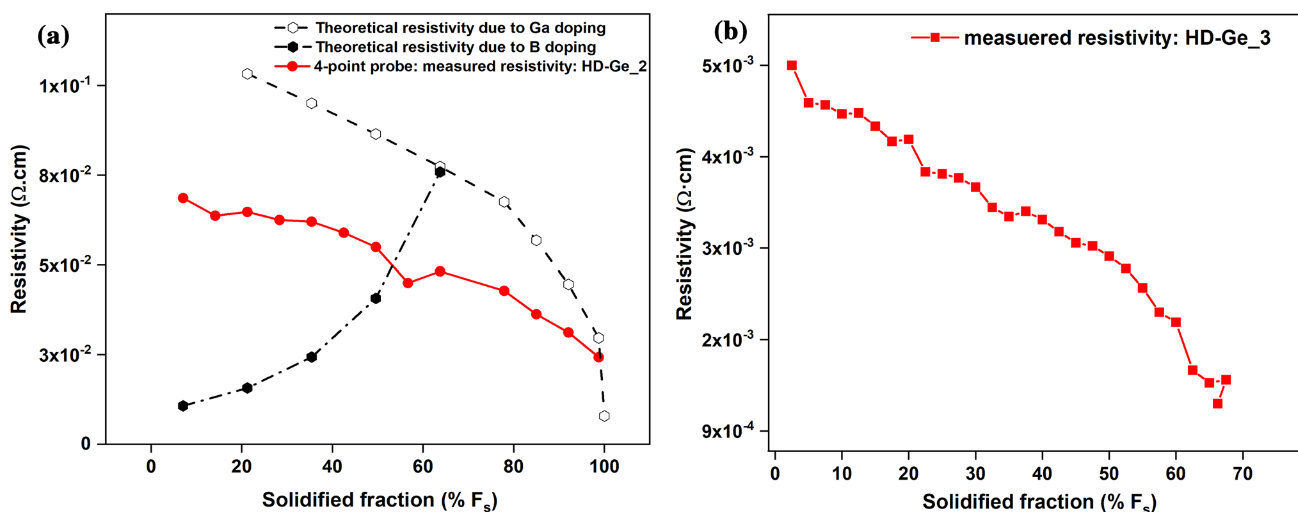

Fig. 9. Resistivity measured using the 4-point probe method for ingot HD-Ge_2 (a) and HD-Ge_3 (b).

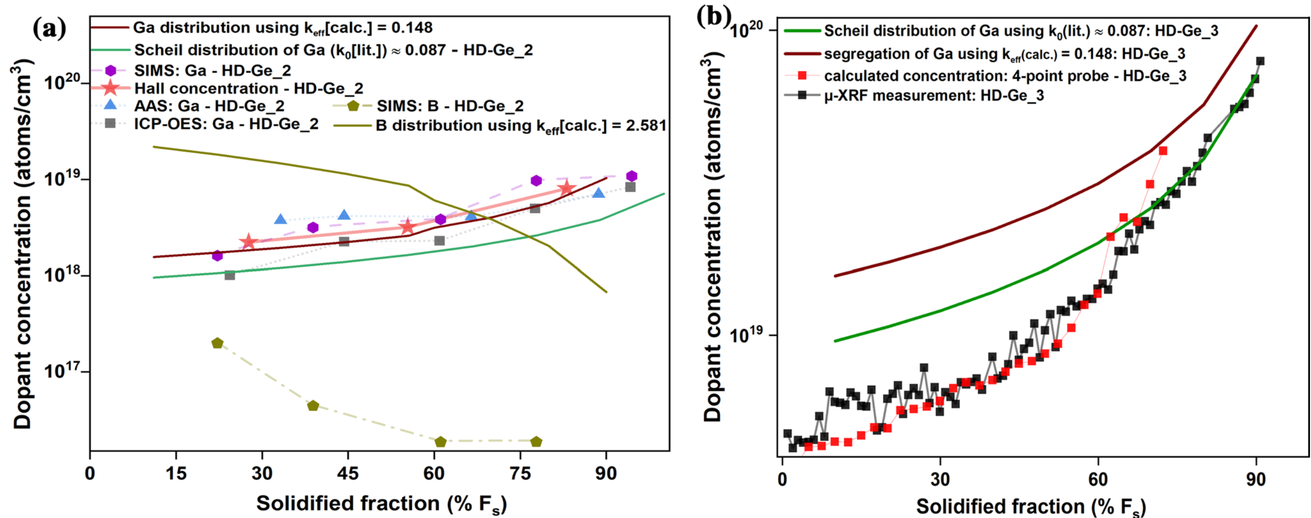

Fig. 10. (a) Measured concentrations of dopants (Ga and B) in HD-Ge_2 by AAS, ICP-OES, SIMS, and Hall measurements versus the distribution of dopants using k_0 from the literature (Scheil distribution) and k_{eff}[calc.] represented in a log scale, (b) measured dopant distribution ingot HD-Ge_3 versus theoretically calculated dopant distribution represented in a log scale.

measured concentration of B at 20% solidified fraction HD-Ge_2 is approximately 8×10^{17} cm^{-3}. Although, the initially doped B (~ 10 cm^{-3}) concentration in HD-Ge_2 was above the reported solubility limit (2×10^{18} cm^{-3}), poly-crystallinity did not occur, which is normally caused due to dopant oversaturation resulting in constitutional supercooling at the crystal–melt interface (for B in Ge, $k_0 \sim 6$).[10,11] Due to the higher concentration of Ga along the entire length of HD-Ge_2, the effect of B in the electrical properties of the ingot is suppressed. One would expect both chemical analytical methods to yield similar results with a negligible difference. On the contrary, AAS measured a higher dopant concentration compared to ICP-OES and Hall measurements in the ingot HD-Ge_2. This is assumed to be because of the tailing of the peaks of ^{70}Ge and ^{71}Ga with the isotopes of Ga (^{69}Ga, and ^{71}Ga) while carrying out ICP-OES.[23] The dopant concentrations measured by μ-XRF were a magnitude lower than the other investigated methods. However, at higher impurity concentrations, μ-XRF measurements followed the Scheil distribution of dopants (Fig. 10b) and match well with the calculated concentration values from the 4-point probe measurement. The resistivity profile from the obtained 4-point probe measurements on ingot HD-Ge_3 corresponds to dopant concentrations between 3×10^{18} and 4×10^{19} atoms/cm^3 (Fig. 10b). The μ-XRF technique could be efficient for characterizing highly doped bulk crystals. In future, standard reference samples with known doping concentrations could be used for cross-reference and to enable a robust and reliable “standard-based” μ-XRF quantification routine.

In efforts to estimate the "actual" experimental effective segregation coefficients (k_{eff}[exp.]) from the growth experiments carried out in this work (see Fig. 11), the following equation has been used,[11,24]

$$C_s = C_0 k_{\text{eff}} \left(1 - F_s\right)^{(k_{\text{eff}}-1)}$$

where C_s and C_0 are the concentration of dopants in the crystal and the initial concentration of dopants in the melt, respectively, and F_s is the solidified fraction of the melt. A large difference in the k_{eff}[exp.] for B in the HD-Ge_2 compared to its k_{eff}[calc.] and k_0(lit.) was observed (Fig, 11b).

The k_{eff}[exp.] of B in HD-Ge_2 was much lower than the k_{eff}[calc.] and the k_0(lit.). This contrast in the segregation coefficients is assumed to be mainly due to the higher concentration of B in the initial Ge melt ($C_0 \approx 10^{19}$ at/cm^3) compared to its solubility limit of B in Ge ($\sim 2 \times 10^{18}$ at/cm^3).[10,11] This reduction in the B incorporation might also be due to its deviation from the vacancy-mediated diffusion mechanism in Ge.[25] The diffusion of B in Ge is reported to be much less than that of Ge self-diffusion. The main mediator of the diffusion process in Ge are the vacancies, as the formation energy of interstitials in Ge is much higher, as in the case of B. This suggests that the diffusion of B may be limited due to the movement of interstitials.[25] Further, the work carried out by Yonenaga[11] suggested the involvement of an electronic effect in the segregation of B in Ge. On the other hand, for the Ga distribution, a slightly higher experimental k_{eff}[exp.] was observed in the co-doped (HD-Ge_2) ingot. The sharp increase in the k_{eff}[exp.] of the Ga in HD-Ge _2 in Fig. 11a reflects the

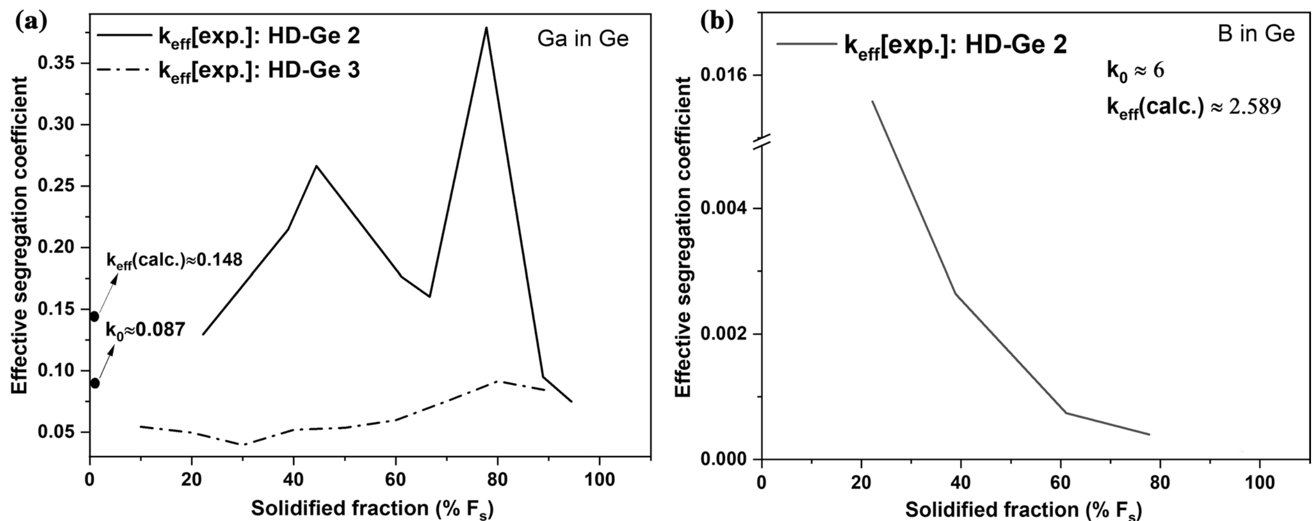

Fig. 11. Experimentally determined effective segregation coefficients of Ga and B in Ge crystals: (a) for Ga in HD-Ge_2 and HD-Ge_3, and (b) for B in a co-doped crystal, HD-Ge_2.

Ga distribution shown in Figs. 9a and 10a. At about 0.5 F_s (in HD-Ge_2) a sharp increase followed by a decrease in the incorporation of dopants is indicated by the measured resistivity profile (as seen in Fig. 9a). A comparable distribution of Ga in HD-Ge_2 was also measured by SIMS (see Fig. 10a). Although the k_{eff}[exp.] of Ga along the crystal length of HD-Ge_2 depicts a non-uniform characteristic, the maximum estimated values were approximately 2 times the k_{eff}[calc.] value of Ga in HD-Ge_2. However, a similar trend was not observed in the Ga-doped HD-Ge_3 ingot (Fig. 11a). Among the possible reasons for the observed increase in Ga segregation in HD-Ge_2, which include the crystal–melt interface properties, and variations in the melt convection, the effect of B-Ga interaction is appealing. Further investigations are ongoing to understand this in detail. Previous literature reports indicate a small increase in the segregation coefficient of Ga in Cz-Si when co-doped with B and Ga. Interestingly, the lower segregation coefficient of B, which was observed in the B-Ga co-doped CZ-Si, was also attributed to the interaction of B and Ga.[26]

Hall measurements were also carried out to determine the active carrier concentrations in the doped ingot (Fig, 12). The Hall concentrations measured in HD-Ge_2 were in agreement with the Ga distribution measured in the ingot. However, there still exists uncertainty in the data obtained from ICP-OES and μ-XRF. Furthermore, post-treatment processes such as annealing could determine if the incorporated dopants can be further activated as opposed to the active carrier concentration measured before annealing (Fig. 12). The concentrations obtained by Hall measurements suggested that the incorporation of dopants in the crystal followed the Scheil-like segregation trend of Ga in Ge.

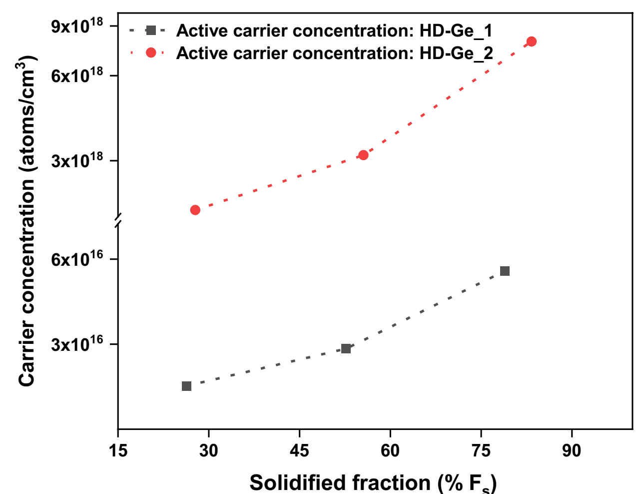

Fig. 12. Hall concentrations of ingots: Ga-doped ingot HD-Ge_1 versus B-Ga-codoped HD-Ge_2 represented in a log scale.

Conclusions

Three doped Ge ingots with different doping levels were grown using the Cz method. Maximum dopant concentrations of up to 5×10^{19} cm^{-3} were achieved in the monocrystalline bulk material. High single crystallinity with XRD-RC FWHM of 9 arcsecs has been observed in ingots with initial doping concentrations up to 10^{19} cm^{-3}. The overall etch pit counts measured in the grown ingots did not show an increase with increasing dopant concentrations. Nevertheless, it has been observed that the number of dislocation clusters increases with higher impurity

concentrations. Furthermore, the presence of a larger number of SAGBs was suggested by the XRD-RC FWHM from HD-Ge_3, which increased with increasing dopant concentration. The aim of co-doping B-and Ga in Ge to obtain a uniform high doping concentration along the entire crystal length could not be achieved, and would need to be tried with further experiments/approaches. The effect of B in the co-doped crystal was not reflected in the resistivity and chemical characterization, as the concentration of Ga along the entire crystal length was higher than that of B. The experimentally obtained values for the effective segregation coefficient, k_{eff}[expt.], of Ga is in good agreement with the literature values. In all the grown crystals, the incorporation of the Ga dopant followed the Scheil predicted distribution. Further understanding of the defect formation and adopting defect cum dopant engineering techniques is crucial to produce highly doped Ge ingots.

Acknowledgments One of the authors (AS) gratefully acknowledges the Director, IKZ, Berlin for providing his support to do PhD work. The authors would like to thank the German Research Foundation (DFG) for the financial support through a research project (grant No.: 509113935). The crystal processing team at IKZ is acknowledged for cutting/polishing the samples. The authors would also like to thank Dr M.D. Huang (The Leibniz-Institut für Analytische Wissenschaften (ISAS)) for carrying out the AAS measurements. Further, the support from Michael Schulze, Pradeep Chandra Palleti, and Palvan Seyidov is acknowledged. A special thanks to Dr. Jens Martin for his critical review of the manuscript.

Funding Open Access funding enabled and organized by Projekt DEAL. This study was funded by the institutional fund of IKZ, Berlin and the German Research Foundation (DFG) (Grant No.: 509113935).

Conflict of interest The authors declare that they have no conflict of interest.

Open Access This article is licensed under a Creative Commons Attribution 4.0 International License, which permits use, sharing, adaptation, distribution and reproduction in any medium or format, as long as you give appropriate credit to the original author(s) and the source, provide a link to the Creative Commons licence, and indicate if changes were made. The images or other third party material in this article are included in the article's Creative Commons licence, unless indicated otherwise in a credit line to the material. If material is not included in the article's Creative Commons licence and your intended use is not permitted by statutory regulation or exceeds the permitted use, you will need to obtain permission directly from the copyright holder. To view a copy of this licence, visit http://creativecommons.org/licenses/by/4.0/.

References

1. G. Pellegrini, L. Baldassare, V. Giliberti, J. Frigerio, K. Gallacher, D.J. Paul, G. Isella, M. Ortolani, and P. Biagioni, Benchmarking the use of heavily doped Ge for plasmonics and sensing in the mid-infrared. *ACS Photon.* 5, 3601 (2018).
2. G.Z. Mashanovich et al., Germanium mid-infrared photonic devices. *J. Lightwave Technol.* 35, 624 (2017).
3. M.P. Fischer et al., Optical activation of germanium plasmonic antennas in the mid infrared. *Phys. Rev. Lett* 117, 047401 (2016).
4. J. Frigerio et al., Tunability of the dielectric function of heavily doped germanium thin films for mid-infrared plasmonics. *Phys. Rev. B* 94, 085202 (2016).
5. J.M. Poumirol et al., Hyper-doped silicon nanoantennas and metasurfaces for tunable infrared plasmonics. *ACS Photon.* 8, 1393 (2021).
6. B. Son, S.H. Shin, Y. Jin, Y. Liao, Z.J. Zhao, J.H. Jeong, Q.J. Wang, X. Wang, C.S. Tan, and M. Kim, A heavily doped germanium pyramid array for tunable optical antireflection in the broadband mid-infrared range. *J. Mater. Chem. C Mater.* 10, 5797 (2022).
7. M.P. Fischer et al., Plasmonic mid-infrared third harmonic generation in germanium nanoantennas. *Light Sci. Appl.* 7, 106 (2018).
8. R.R. Sumathi, N. Abrosimov, K.P. Gradwohl, M. Czupalla, and J. Fischer, Growth of heavily-doped germanium single crystals for mid-infrared applications. *J. Cryst. Growth* 535, 125490 (2020).
9. R. Singh, A.F. Witt, and H.C. Gatos, Oscillatory interface instability during Czochralski growth of heavily doped germanium. *J. Electrochem. Soc.* 121, 380 (1974).
10. O. Madelung, M. Schulz, and H. Weiss, *Landolt-Börnstein: numerical data and functional relationships in science and technology*, Vol. 17 (Springer, 1984).
11. I. Yonenaga, Germanium crystals, *Single crystals of electronic materials: growth and properties*. ed. F. Roberto (Elsevier, 2018), pp. 89–127.
12. C. Guguschev, R. Tagle, U. Juda, and A. Kwasniewski, Microstructural investigations of $SrTiO_3$ single crystals and polysilicon using a powerful new x-ray diffraction surface mapping technique. *J. Appl. Cryst* 48, 1883 (2015).
13. S. Wagner, IEEE standard test procedures for high-purity germanium crystals for radiation detectors. *IEEE Std1160* 1993, 11 (1993).
14. J. Sherman, The theoretical derivation of fluorescent x-ray intensities from mixtures. *Spectrochim. Acta* 7, 283 (1955).
15. W.L. Hansen, R.H. Pehl, E.J. Rivet, and F.S. Goulding, Selection of germanium for lithium-drifted radiation detectors by observation of etch-pit distributions*. *Nucl. Instrum. Methods* 80, 181 (1970).
16. E. Billig, Some defects in crystals grown from the melt-I defects caused by thermal stresses. *Proc. R Soc. Lond. A Math. Phys. Sci.* 235, 37 (1956).
17. D.B. Cuttriss, Relation between surface concentration and average conductivity in diffused layers in germanium. *Bell Syst. Tech. J.* 40, 509 (1961).
18. J.A. Burton, R.C. Prim, and W.P. Slichter, The distribution of solute in crystals grown from the melt. Part I. Theoretical. *J. Chem. Phys.* 21, 1987 (1953).
19. E. Scheil, Bemerkungen Zur Schichtkristallbildung. *Z. Met.* 34, 70 (1942).
20. A.G. Ostrogorsky, and G. Muller, A model of effective segregation coefficient, accounting for convection in the solute layer at the growth interface. *J. Cryst. Growth* 121, 587 (1992).
21. J.A. Burton, E.D. Kolb, W.P. Slichter, and J.D. Struthers, Distribution of solute in crystals grown from the melt. Part II. Experimental. *J. Chem. Phys.* 21, 1991 (1953).
22. T. Taishi, Y. Murao, Y. Ohno, and I. Yonenaga, Segregation of Boron in germanium crystal. *J. Cryst. Growth* 311, 59 (2008).
23. M. Niemelä, H. Kola, and P. Perämäki, Determination of trace impurities in germanium dioxide by icp-oes, icp-ms and etaas after matrix volatilization: a long-run performance of the method. *Anal. Sci.* 30, 735 (2014).
24. W.G. Pfann, Principles of zone-melting. *J. Miner. Met. Mater. Soc. (TMS)* 4, 747 (1952).
25. A. Chroneos, and H. Bracht, Diffusion of n -type dopants in germanium. *Appl. Phys. Rev.* 1, 011301 (2014).

26. X. Huang, M. Arivanandhan, R. Gotoh, T. Hoshikawa, and S. Uda, Ga segregation in Czochralski-Si crystal growth with B codoping. *J. Cryst. Growth* 310, 3335 (2008).

Publisher's Note Springer Nature remains neutral with regard to jurisdictional claims in published maps and institutional affiliations.